TiO_2/EVOH based reactive interlayer in Surlyn for organic device encapsulation

Materials Research Express

PAPER

TiO_2/EVOH based reactive interlayer in Surlyn for organic device encapsulation

RECEIVED
26 September 2015

REVISED
20 October 2015

ACCEPTED FOR PUBLICATION
12 November 2015

PUBLISHED
14 January 2016

Gayathri N Kopanati[1], **Praveen C Ramamurthy**[2,3] **and Giridhar Madras**[1]

[1] Department of Chemical Engineering, Indian Institute of Science, Bangalore, 560012, India
[2] Centre for Nanoscience and Engineering, Indian Institute of Science, Bangalore, 560012, India
[3] Department of Materials Engineering, Indian Institute of Science, Bangalore, 560012, India

E-mail: giridhar@chemeng.iisc.ernet.in

Keywords: polymer nanocomposite, barrier materials, encapsulation, water vapor transmission

Abstract

Barrier materials are important for improving the stability and lifetimes of organic electronic devices. A simple technique for improving the barrier properties of polymer films was considered in this work by using TiO_2 nanoparticles in the interlayer to be incorporated in the polymer film. TiO_2 was synthesized by the solution combustion technique, was further functionalized using stearic acid or octadecylamine to induce hydrophobicity and enhance processing of the composite interlayer. The grafting of these compounds on to TiO_2 was investigated using Fourier transform infrared spectroscopy, Raman spectroscopy, elemental analysis and thermo-gravimetric analysis. The functionalized and neat TiO_2 were blended with poly (vinyl alcohol-ethylene) (EVOH) and were melt compressed between Surlyn films. The resulting nanocomposite films were tested for their transparency and barrier properties using UV–visible spectroscopy and calcium degradation test, respectively. Further, the effectiveness of these barrier films in encapsulating organic devices was determined from accelerated aging tests. Therefore, the synthesized barrier films with neat and functionalized TiO_2 in the interlayers proved to be effective as moisture barrier composite films.

1. Introduction

The drive to produce flexible electronic devices paved the path for the development of organic electronics [1–4]. Unlike their inorganic counterparts, these devices are flexible and also offer the advantage of solution processing [5, 6]. These devices can be fabricated using simple and economical techniques such as roll-to-roll processing [7, 8]. However, the long term stability of organic thin films is a hindrance for the commercialization of these devices. The conducting organic layers degrade in the presence of oxygen and moisture and undergo photo oxidation [9–12]. Low work function electrodes utilized by these devices are reactive to moisture resulting in loss of electronic properties and delamination [13–15]. The water vapor transmission rates (WVTR) should be as low as 10^{-6} g m^{-2} d^{-1} for increased lifetimes and stability of organic devices [16, 17]. Therefore, encapsulation of these sensitive devices is critical for their efficient functioning.

Glass can be a direct solution for encapsulation as it possess major requirements of an encapsulant such as transparency, impermeability to moisture and oxygen, and stability [16]. The main drawback with glass is its inflexibility. Though flexible glass can now be fabricated using down-draw processing [18, 19], it cannot be used as encapsulants because it is brittle. Plastic materials used as gas/moisture barriers in food and pharmaceutical industries are flexible. However, these materials cannot provide the stringent levels of water vapor barrier that are required for organic device encapsulation [20, 21]. Thin metal foils and organic/inorganic layered barriers are flexible and can be developed with required permeation rates. However, pinhole mediated permeation of moisture and their opacity makes them unsuitable for encapsulation [19, 22]. Therefore, the development of barrier materials that are flexible, transparent and with the required water vapor permeabilities is crucial for the commercialization of organic devices. In order to develop a suitable barrier material possessing all these

properties, barrier materials based on reactive nanocomposites such as MgO have been recently being investigated [23, 24].

Nanocomposites are synthesized by incorporating nanoparticles into the polymer matrix to develop reinforced and high performance materials. The addition of nanomaterials to polymer resin would enhance the properties of matrix such as electrical conductivity, elasticity, insulation, mechanical strength, thermal stability and gas barrier [25–29]. These properties can be achieved at extremely low concentrations of nanoparticles because the interactions at the particle/matrix interface will be largely improved at nanoscale compared to macro or micro scale. Moisture barrier properties of various nanocomposites such as Al_2O_3, ZnO and SiO_2 have been recently investigated [30–32]. Polymer nanocomposites also find their applications in biomaterials [33, 34], sensors [35] and while their use as gas barrier materials have gained a lot of interest due to their direct implications in packaging [36, 37]. The finely dispersed nanoparticles in the polymer matrix create a tortuous path for permeating gas molecules thereby increasing the diffusion path length and time of these molecules. This will result in decreased permeation rates of gas molecules [38]. The decrease in permeation rates is further governed by factors like dispersion, aspect ratio, and volume fraction of the nanoparticles [39, 40].

The WVTRs can be further reduced if the permeating water molecules can chemically bond or interact with the nanoparticles. However, this aspect of polymer nanocomposites is less studied and reported compared to non-reactive nanocomposites. Further, composites based on titania have not been reported earlier. In this study, a polymer nanocomposite with titanium oxide (TiO_2) nanoparticles was developed. The neat TiO_2 nanoparticles have the ability to form hydroxyl bonds with the permeating water molecules enhancing the barrier property of the nanocomposite films. Further, the TiO_2 was surface modified to study the effect of grafting on water vapor permeability.

TiO_2 particles were synthesized following solution combustion technique, a method which is widely used to synthesize metal oxides [41, 42]. The solution combustion method to synthesize TiO_2 so that the size of the nanoparticles was <10 nm. This low size of the nanoparticles ensures higher reactivity and the surface modification of these nanoparticles resulted in better dispersion in terms of the time required for dispersing and obtaining composites with lesser agglomeration. Further, this method is preferred over other techniques because it is comparatively simple, easy to handle, economical, can be processed at low temperatures and results in the product with lower particle size and higher defect sites. The lower particle size ensures higher surface area while the higher defect sites in increasing the reactivity. TiO_2 was previously synthesized using fuels like glycine, triethyl amine, and hexamine [43, 44]. In this study, TiO_2 was synthesized using lactose and surface modified using a carboxylic acid and an amine to improve the dispersion of TiO_2 in the polymer and to study the effect of surface modification on the water vapor permeability. TiO_2 synthesized using solution combustion is hydrophilic and grafting stearic acid and octadecylamine on to the surface of TiO_2 will impart hydrophobicity.

Therefore, the objective of this work was to synthesize an interactive polymer nanocomposite as water vapor barrier for encapsulation of organic devices. Pristine and functionalized TiO_2 was blended with poly (vinyl alcohol-co-ethylene) (EVOH). To further enhance the water vapor barrier of EVOH nanocomposites films, these films were sealed between two Surlyn films. The synthesized nanoparticles and nanocomposite films were characterized using various techniques and the WVTRs were determined using calcium degradation test. Further, accelerated aging tests were used to evaluate the performance of organic photovoltaics (OPVs) encapsulated with fabricated barrier films under accelerated weathering conditions.

2. Materials and methods

Titanium (IV) isopropoxide (TISO) was obtained from Alfa Aesar (USA). Lactose was purchased from Fischer Scientific (India). Poly (vinyl alcohol-co-ethylene) (EVOH) with 38% ethylene (in mol), octadecylamine (ODA), Poly (ethylene-co-methacrylic acid), Surlyn (zinc salt), PEDOT-PSS, [6, 6]-phenyl-C_{61}-butyric acid methyl ester (PCBM) calcium metal ($\sim$99.99% purity) and stearic acid were procured from Sigma Aldrich Chemical Company, Inc. (USA). Nitric acid and hydrogen peroxide were obtained from Merck. Dimethyl sulfoxide (DMSO), used as solvent, was obtained from S.D. fine chemicals (India). Poly (3-hexylthiophene) (P3HT) was purchased from Rieke Metals Inc. (USA). The epoxy glue used for sealing the barrier films was obtained from Atul Industries Ltd (India).

2.1. Synthesis of TiO_2 nanoparticles

TiO_2 was prepared following the solution combustion technique. Titanyl nitrate was synthesized using TISO [43]. TISO was added drop wise to ice cold water under continuous stirring. The titanyl hydroxide ($TiO(OH)_2$) precipitate was filtered out and washed thoroughly. The powder of $TiO(OH)_2$ was slowly added to 1:2 nitric acid and water solution. The mixture was stirred continuously till a clear transparent solution of titanyl nitrate was

obtained. Thus obtained solution was used for solution combustion by mixing titanyl nitrate (oxidizer) and lactose (fuel) in their stoichiometric molar ratios and this mixture was combusted at 350 °C in a muffle furnace.

2.2. Surface modification of TiO_2

2.2.1. Amine functionalization

The ODA and synthesized TiO_2 taken in the molar ratio of 2:1 were dispersed in toluene by ultra-sonication. The dispersed solution was refluxed at 120 °C for 36 h under nitrogen atmosphere. The resulting powder was washed several times with toluene to remove unreacted ODA. The surface modified TiO_2 was dried in a vacuum oven at 110 °C for 4 h to remove toluene [45].

2.2.2. Acid functionalization

SA and TiO_2 nanoparticles in molar ratio of 2:1 were dispersed in toluene. This mixture was refluxed at 120 °C for 36 h. The product obtained was vacuum filtered at 110 °C for 4 h to remove toluene. Thus obtained TiO_2, grafted with SA and ODA will be referred as SA-TiO_2 and ODA-TiO_2, respectively [46].

2.3. Fabrication of barrier samples

Polymer nanocomposites of EVOH and TiO_2 were prepared by solution processing technique. EVOH was added to DMSO and stirred at 80 °C using a magnetic stirrer until the polymer completely dissolved in the solvent. Various weight % of neat TiO_2 and surface modified TiO_2 (0.5%–3%) were added to the polymer solution and stirred till a finely dispersed solution was obtained. Deionized water was added to the above polymer solution that resulted in the formation of white precipitate of polymer nanocomposite. The precipitate was vacuum filtered and dried at 60 °C for 20 h to evaporate DMSO and water. The dried product was compression molded at 190 °C to obtain composite films of thickness ~75 μm. These films were then sealed between two Surlyn films (of ~50 μm each) by thermal treatment to finally obtain the barrier films of thickness ~150 μm. Unless otherwise mentioned, nanocomposites films with 2% loading were used for further analyses.

2.4. Methods

Rigaku SmartLab, x-ray diffractometer (XRD) was used to determine the phase and crystallite size of the synthesized TiO_2 nanoparticles. The powder was scanned at a scan rate of 1° min^{-1} over a 2Θ in the range: 25°–85°. The surface areas and pore volumes of synthesized and functionalized TiO_2 were determined using BET (Smartsorb, India). Perkin Elmer FTIR/FIR frontier spectrometer was used to characterize the synthesized neat TiO_2 and functionalized TiO_2 in the range of 4000 to 400 cm^{-1} by accumulating 32 scans at a resolution of 4 cm^{-1}. Raman spectroscopy (Lab Ram HR) and x-ray photoelectron spectroscopy (Thermo Scientific Multilab 2000) were used to confirm the grafting of SA and ODA on to the TiO_2 surface. LECO TruSpec (CHN) and Perkin Elmer thermogravimetric analyzer (TGA) were further used to determine the grafting density of surface modifiers, SA and ODA. The optical transparency of polymer nanocomposite films over the range of 230–1100 nm was determined using Perkin Elmer (Lambda 35) UV–visible spectroscophotometer.

2.5. Permeability studies

Calcium degradation test, which is a technique used to determine water vapor permeabilities through the barrier materials, was used to calculate WVTR through the synthesized barrier films. In this test, the change in conductance for the sealed calcium thin film with the barrier sample is monitored with time. The conductance decreases with time due to the oxidation of calcium when it comes in contact with water vapor. Thus the amount of water permeated is related to the amount of calcium oxidized and is used for determining WVTR through the barrier films following the standardized setup [47].

2.6. OPV device aging studies

The effectiveness of the fabricated film to encapsulate an OPV device under accelerated weathering conditions is determined from accelerated device aging studies. OPV devices were fabricated using an indium tin oxide (ITO) coated glass slide with active layers of PEDOT-PSS and P3HT-PCBM and used for this study. ITO coated glass slides were etched on the two edges. PEDOT-PSS was spin coated at 3000 rpm for 1 min followed by annealing at 110 °C for 10 min P3HT (22 mg) and PCBM (18 mg) in 1 ml of dichlorobenzene was spin coated on the glass slides and annealed at 140 °C for 10 min. Aluminum (electrodes) was thermally evaporated on to the etched edges of the glass slides to provide contacts for measurements. These devices were sealed with the synthesized barrier films and subjected to accelerated weathering conditions (RH = 85% and 65 °C) and efficiencies of the devices was determined using a Keithley semiconductor characterization system (4200) and the solar simulator (sol 3 A, Newport Oriel) [23].

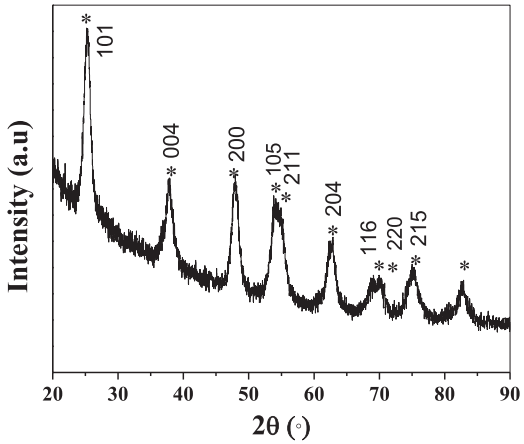

Figure 1. Powder XRD pattern of nano TiO_2 synthesized through solution combustion technique.

3. Results and discussion

The Surlyn barrier films were fabricated with EVOH interlayer containing the synthesized neat and functionalized TiO_2 nanoparticles. The process of dispersion of neat TiO_2 in EVOH was found to be relatively difficult due to agglomeration when compared to the surface modified TiO_2. SA and ODA were grafted on to the surface of TiO_2 nanoparticles for surface modification. The hydroxyl groups present on the surface of TiO_2 nanoparticles will react with the carboxyl group of SA and amine group of ODA [46]. This results in the formation of surface modified TiO_2 nanoparticles with dangling hydrophobic carbon chains [45, 46], which help in the formation of better dispersion with polymers. Polymer nano-composites generally offer better gas barrier properties due to the increase in the tortuosity for permeation [38]. Further, the addition of moisture reactive components to the polymer would result in the enhancement of barrier properties.

3.1. Characterization of the synthesized nanoparticles

3.1.1. XRD studies

The XRD pattern for nanoparticles obtained from combustion synthesis is given in figure 1. The diffraction data shows the formation of TiO_2 (JCPDS 00-001-0562) with characteristic peaks of TiO_2 at $2\Theta = 25.275°, 37.7°, 48.0°, 55.27°, 62.6°, 70.17°, 75.23°$ and $83°$. These peaks refer to the formation of pure anatase phase. Further, the crystallite size for the synthesized TiO_2 calculated using Scherrer formula is ~7 nm.

3.1.2. FTIR and Raman spectroscopic analyses

The FTIR spectra for pristine and surface modified TiO_2 are given in figure 2(a). The broad peak in the range of 3500–3200 cm^{-1} in pristine TiO_2 is due to the –OH stretching of hydroxyl groups bonded to TiO_2 nano particles [48]. Similarly, the peak at ~1640 cm^{-1} can be ascribed to –OH bending vibrations. The absence of these peaks in functionalized TiO_2 suggests that there is reaction of carboxylic acid group of SA and amine group of ODA with the hydroxyl groups on TiO_2. After functionalization, there were additional peaks observed at ~2910 and 2848 cm^{-1} which are characteristic to symmetric and asymmetric –CH stretchings [48], respectively.

The peaks at ~1550 and 1400 cm^{-1} in SA-TiO_2 can be attributed to –COO symmetric and asymmetric vibrations [46]. The small peak at ~1630 cm^{-1} in ODA-TiO_2 can be ascribed to -NH bending. Therefore, these peaks confirm the presence of –COOH and $–NH_2$ of SA and ODA respectively. Further, in order to confirm the grafting of these functional groups on the synthesized TiO_2, Raman spectra were given in figures 2(b) and (c). The bands observed in samples SA-TiO_2 and ODA-TiO_2 at ~2800 cm^{-1} are due to the presence of –CH groups [45]. The peaks at 144 cm^{-1} are characteristic of the anatase TiO_2 groups. From figure 2(c), it can be observed the peak at 144 cm^{-1} was shifted towards lower wavenumbers in the case of functionalized TiO_2. Therefore, this shift in the wavelength confirms that SA and ODA are grafted on to the surface of TiO_2.

3.1.3. Surface area analysis

The BET surface area based on nitrogen adsorption–desorption for the synthesized TiO_2 was found to be 160 $m^2\ g^{-1}$. The high surface area of nanoparticles is due to its high porous structure with the pore volume of 0.85 $cm^3\ g^{-1}$. The surface areas for both SA and ODA functionalized TiO_2 were found to be ~29 and 10 $m^2\ g^{-1}$, respectively and the pore volumes were found to be ~0.3 $cm^3\ g^{-1}$ for SA and ODA functionalized TiO_2. This drastic reduction in pore volumes and surface area indicate the effective functionalization of nanoparticles.

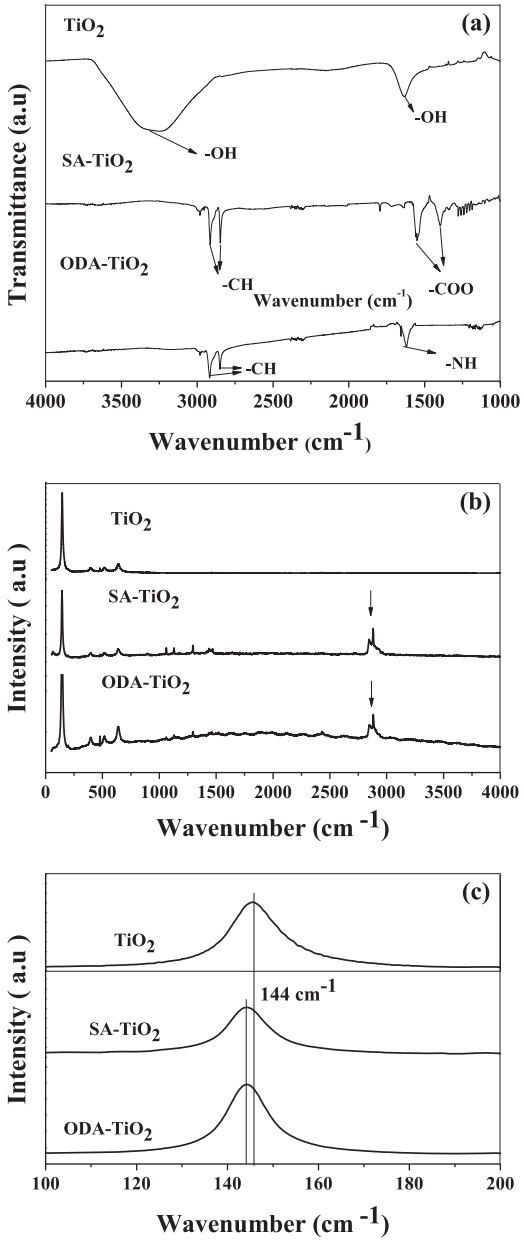

Figure 2. (a) FTIR, (b) and (c) Raman spectra of neat and functionalized TiO_2.

3.1.4. Elemental analysis

The elemental and thermal analyses of pristine and functionalized TiO_2 were used to quantify the grafting of SA and ODA over the surface of TiO_2. The increase in carbon, nitrogen and hydrogen percentages of nanoparticles after functionalization prove that SA and ODA were grafted on to the TiO_2 surface. The C, H and N percentages and BET surface area of pristine TiO_2 are used to calculate grafting density of SA and ODA on the surface of TiO_2. The percentage of carbon in TiO_2, SA-TiO_2 and ODA-TiO_2 is 0.3175%, 10.25% and 45.89%, respectively. The hydrogen percentage for samples TiO_2, SA-TiO_2 and ODA-TiO_2 is 1.06%, 1.78% and 7.65%, respectively, while the nitrogen percentage in ODA-TiO_2 is 3.68%.

$$Q^{CH} = \frac{d_c}{M_C \times N_C \times A}. \quad (3)$$

In equation (3), d_c is the % increase in carbon content obtained from CHN analysis, M_C is the atomic weight of carbon, N_C number of carbon atoms on the surface of TiO_2 and A is the surface area of neat TiO_2 from BET [49]. The grafting density for SA and ODA calculated using equation (3) are ~2.8 (~2 nm^{-2}) and 13.9 (~8.5 nm^{-2}) μmol m^{-2}, respectively. Considering –OH coverage over the surface of TiO_2 to be ~14 nm^{-2}, the surface coverage determined from CHN analysis is ~18% and 71% for SA and ODA, respectively [50].

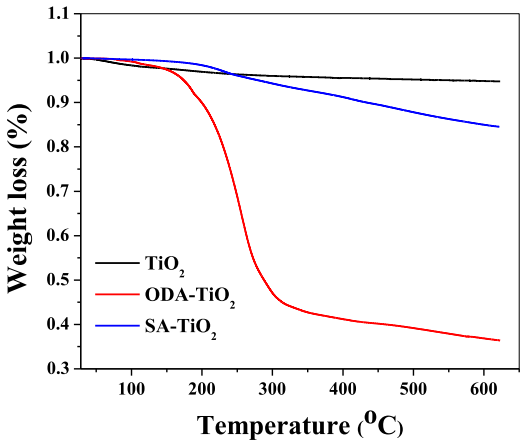

Figure 3. Weight loss of pristine and functionalized TiO_2 obtained from TGA.

3.1.5. Thermogravimetric analysis

The weight loss for neat and functionalized TiO_2 over the temperature of 25 °C–650 °C is given in figure 3. The weight loss observed from 25 °C to 150 °C for functionalized sample while the weight loss in the range of 25 °C–650 °C for neat samples is mainly due to water molecules adsorbed on the surface. Further loss from 150 °C to 650 °C for functionalized TiO_2 is due to the degradation of grafted SA and ODA on the surface of TiO_2 [49]

$$Q^{\mathrm{TGA}} = \frac{W}{M \times A}. \tag{4}$$

In equation (4), W is the % weight loss determined from TGA analysis, M is the molecular weight of organic molecules grafted to the surface of TiO_2 and A is the surface area of TiO_2 from BET. The weight loss from 160 °C to 650 °C for SA and ODA grafted TiO_2, as observed from figure 3, is ∼16% and 71%, respectively. The grafting density calculated using equation (4) are ∼3.2 (∼2 nm^{-2}) and 13.2 (∼11.4 nm^{-2}) μmol m^{-2} [49]. Therefore, the surface coverage of SA and ODA is ∼15% and 81%, respectively. Further, it can be inferred from the TGA and CHN analysis that the grafting density of ODA is nearly three times higher than that of SA. The BET surface area of SA-TiO_2 is higher than ODA-TiO_2 implying that the surface coverage of ODA is higher compared to SA.

3.2. Composite film characterization

3.2.1. UV visible analysis

The optical transparency, which is one of the important features of an encapsulant, is evaluated by UV–visible spectroscopy. The average transmittance obtained in the range of 200–800 nm for all the nanocomposite films with different loadings is given in figure 4. It can be observed that the optical transparency decreases with increase in loading. The films have similar transparency at 0.5% and 1% filler concentration. The transparency of 2% neat TiO_2 nanocomposite is lower compared to that of functionalized TiO_2. However, the average transmittance for all the composite films is ⩾50%, which is acceptable for encapsulation applications [51].

3.3. Permeability studies

Extensive details on the determination of WVTR from calcium degradation studies are given in our previous studies [45, 47, 49]. The water vapor permeabilities obtained from calcium degradation test for the nanocomposite films at ∼4000 s are shown in figure 5. The WVTR of neat TiO_2 nanocomposites decrease with increase in filler concentration from 0.5% to 1%. However, there is ∼5.5 times increase in WVTR with 2% when compared to 1% loading for neat TiO_2 nanocomposites and the performance of the nanocomposites with 3% neat TiO_2 is poor and the WVTR is lesser than that obtained with 0.5% loading. The increase of WVTR at higher loadings is due to agglomeration of TiO_2. Thus, functionalization of TiO_2 would be helpful as it would prevent agglomeration. This is apparent from the WVTR studies. When dealing with functionalized TiO_2, the WVTRs increases continuously with increasing loading of modified TiO_2 and the WVTR of 3% functionalized TiO_2 is significantly lesser than that obtained with 1% functionalized TiO_2. Further, the barrier films with interlayers comprising TiO_2 modified with SA exhibited better water vapor barrier performance than the films with ODA modified TiO_2. This could be attributed to the higher grafting of ODA on to TiO_2 resulting in the complete surface coverage of TiO_2. Therefore, the dispersed TiO_2 is unavailable for reacting with permeating moisture, resulting in higher WVTRs when compared to SA-TiO_2 barrier films .

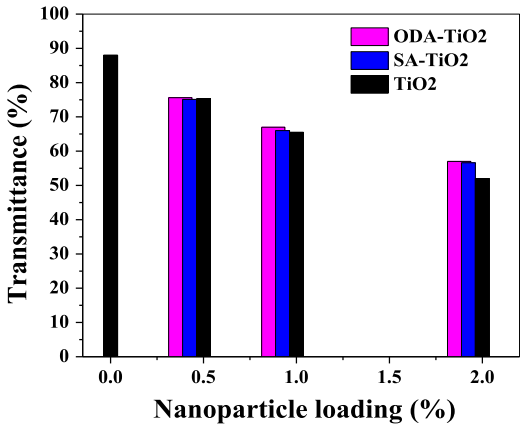

Figure 4. Average visible light transparency of the barrier films with various filler loadings.

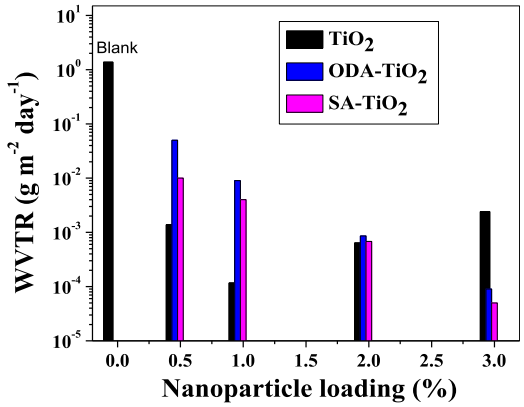

Figure 5. WVTR of nanocomposite films at ~4000 s for different TiO_2 loadings.

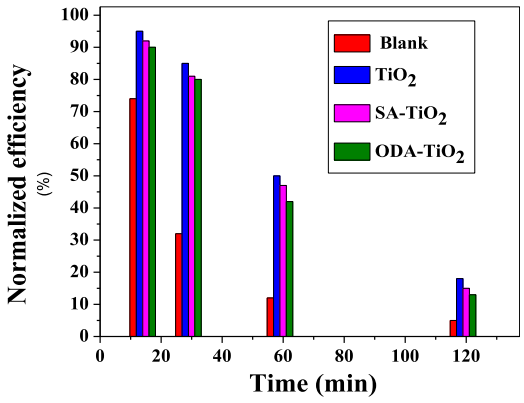

Figure 6. Normalized efficiency of 2% nanocomposites subjected to accelerated weathering conditions for various time periods.

3.4. Accelerated aging studies

The OPV devices were encapsulated with the fabricated barrier films (2% loading) to study the effectiveness of EVOH/TiO_2 interlayers for organic device encapsulation. When devices were subjected to accelerated aging conditions, the performances of the devices decreased with time (figure 6) due to the permeation of moisture through the encapsulation. In the case of barrier films without TiO_2 in the interlayer, the efficiency dropped down to 74%, 32%, 12% and 5% of its initial performance in 15, 30, 60 and 120 min, respectively. When the interlayer was dispersed with neat TiO_2, SA-TiO_2 and ODA-TiO_2, the efficiencies were found to be 95%, 92%

and 81% after 15 min, 85%, 81% and 80% after 30 min, 50%, 47% and 42% after 60 min and 18%, 15% and 13% after 120 min of accelerated aging, respectively. These results suggest that the composites with interlayers comprising TiO_2 are better encapsulants than those without TiO_2. Among the interlayers with TiO_2, the neat TiO_2 exhibited better barrier properties than the surface modified TiO_2 due to the availability of more surface area for interacting with the permeating H_2O molecules. Similarly, the devices encapsulated with barrier films containing SA-TiO_2 interlayers sustained with higher efficiencies due to the lower surface coverage when compared to the barrier films with ODA-TiO_2. Therefore, these results are in agreement with the previously studied WVTRs through the composites. Further, these accelerated aging studies suggest that the synthesized composite films can sustain the performance of the devices up to ∼50% for ∼1 h. This clearly shows that the synthesized barrier films are capable of sustaining the device lifetimes under ambient conditions at 25 °C and 35% RH for ∼1000 h [52].

4. Summary and conclusions

The Surlyn/EVOH(with neat or modified TiO_2)/Surlyn barrier architectures were studied for organic device encapsulation. The TiO_2 used in the work has been synthesized by solution combustion technique to obtain nanoparticles with high surface areas. The synthesized nanoparticles were characterized and then used for synthesizing the composite films with EVOH. Due to the difficulty in achieving proper dispersion of TiO_2 in EVOH, the TiO_2 nanoparticles were functionalized with SA and ODA. The extent of surface modification was determined from elemental and thermal analyses suggesting higher surface coverage in the case of ODA-TiO_2 when compared to SA-TiO_2. Further, the EVOH composite films fabricated using these functionalized and neat TiO_2 were subjected to visible light transparency and water vapor barrier studies. All the transparencies were above 50% indicating these are suitable for encapsulation applications. However, the key property that determines the application of these materials for encapsulation is the WVTR. The polymer nanocomposite films without TiO_2 exhibited WVTR of ∼1 g m^{-2} day^{-1}. Incorporating neat TiO_2 in the nanocomposite resulted in reduced WVTR of $\sim 10^{-4}$ g m^{-2} d^{-1}. The higher barrier properties of the composite films with neat TiO_2 were attributed to the high surface area and porosity of TiO_2 nanoparticles. The WVTR reduced with increasing TiO_2 content up to 1% loading but decreased on further loading due to agglomeration. In the case of SA and ODA modified TiO_2, the WVTRs decreased with increasing loading and reduced WVTR of $\sim 10^{-5}$ g m^{-2} d^{-1} was achieved with 3% loading. The composites investigated in this study showed WVTRs that are considerably lower than the WVTRs of ∼0.015, 0.0089 and 0.07 g m^{-2} d^{-1} obtained with the composites of Al_2O_3, ZnO and SiO_2, respectively [30–32]. This indicates that the composites with TiO_2 exhibited superior barrier properties. The SA-TiO_2 composite films exhibited better moisture barrier properties than the ODA-TiO_2 composites. Further, the accelerated aging studies for the encapsulated OPV devices suggest the effectiveness of the barrier films by improving the device lifetimes.

Acknowledgments

The authors would like to acknowledge the wonderful help and discussion provided by Dr Sindhu Seethamraju. The authors also thank SERB, Department of Science and Technology (DST/1362/2014) for the financial support for this project. The corresponding author thanks DST for the J C Bose fellowship.

References

[1] Ramamurthy P C, Malshe A M, Harrell W R, Gregory R V, McGuire K and Rao A M 2004 Polyaniline/single-walled carbon nanotube composite electronic devices *Solid-State Electron.* **48** 2019–24
[2] Bundgaard E and Krebs F C 2007 Low band gap polymers for organic photovoltaics *Sol. Energy Mater. Sol. Cells* **91** 954–85
[3] Brabec C J, Sariciftci N S and Hummelen J C 2001 Plastic solar cells *Adv. Funct. Mater.* **11** 15–26
[4] Ramamurthy P, Harrell W and Gregory R 2003 Influence of N, N′ dimethylpropyleneurea content in polyaniline on electrical characteristics and device performance *Electrochem. Solid-State Lett.* **6** G113–6
[5] Lewis J 2006 Material challenge for flexible organic devices *Mater. Today* **9** 38–45
[6] Brabec C J and Durrant J R 2008 Solution-processed organic solar cells *MRS Bull.* **33** 670–5
[7] Krebs F C 2009 All solution roll-to-roll processed polymer solar cells free from indium-tin-oxide and vacuum coating steps *Org. Electron.* **10** 761–8
[8] Søndergaard R R, Hösel M and Krebs F C 2013 Roll-to-Roll fabrication of large area functional organic materials *J. Polym. Sci.* B **51** 16–34
[9] Cumpston B H, Parker I D and Jensen K F 1997 *In situ* characterization of the oxidative degradation of a polymeric light emitting device *J. Appl. Phys.* **81** 3716–20
[10] Günes S, Neugebauer H and Sariciftci N S 2007 Conjugated polymer-based organic solar cells *Chem. Rev.* **107** 1324–38
[11] Low H Y 2002 Photo and photo-oxidative degradations of poly(phenylene vinylene) derivatives *Thin Solid Films* **413** 160–6
[12] Sutherland D G J *et al* 1996 Photo-oxidation of electroluminescent polymers studied by core-level photoabsorption spectroscopy *Appl. Phys. Lett.* **68** 2046–8

[13] Hoppe H and Sariciftci N S 2004 Organic solar cells: an overview *J. Mater. Res.* **19** 1924–45
[14] Jørgensen M, Norrman K and Krebs F C 2008 Stability/degradation of polymer solar cells *Sol. Energy Mater. Sol. Cells* **92** 686–714
[15] Kawano K and Adachi C 2009 Evaluating carrier accumulation in degraded bulk heterojunction organic solar cells by a thermally stimulated current technique *Adv. Funct. Mater.* **19** 3934–40
[16] Dennler G, Lungenschmied C, Neugebauer H, Sariciftci N, Latreche M, Czeremuszkin G and Wertheimer M 2006 A new encapsulation solution for flexible organic solar cells *Thin Solid Films* **511** 349–53
[17] Lewis J S and Weaver M S 2004 Thin-film permeation-barrier technology for flexible organic light-emitting devices *IEEE J. Sel. Top. Quantum Electron.* **10** 45–57
[18] Plichta A, Weber A and Habeck A 2003 Ultra thin flexible glass substrates *MRS Proceedings* (Cambridge: Cambridge University Press) p H9. 1
[19] Crawford G 2005 *Flexible Flat Panel Displays* (New York: Wiley)
[20] Siracusa V, Rocculi P, Romani S and Dalla Rosa M 2008 Biodegradable polymers for food packaging: a review *Trends Food Sci. Technol.* **19** 634–43
[21] Sorrentino A, Gorrasi G and Vittoria V 2007 Potential perspectives of bio-nanocomposites for food packaging applications *Trends Food Sci. Technol.* **18** 84–95
[22] Seethamraju S, Rao A D, Ramamurthy P C and Madras G 2014 Layer-by-layer assembly of nafion on surlyn as ultra-high water vapor barrier material *Langmuir* **30** 14606
[23] Kopanati G N, Seethamraju S, Ramamurthy P C and Madras G 2015 A Surlyn/magnesium oxide nanocomposite as an effective water vapor barrier for organic device encapsulation *RSC Adv.* **5** 32580–7
[24] Cho E S, Evans C M, Davidson E C, Hoarfrost M L, Modestino M A, Segalman R A and Urban J J 2015 Enhanced water vapor blocking in transparent hybrid polymer–nanocrystal films *ACS Macro Lett.* **4** 70–4
[25] Kim H, Miura Y and Macosko C W 2010 Graphene/polyurethane nanocomposites for improved gas barrier and electrical conductivity *Chem. Mater.* **22** 3441–50
[26] Choudalakis G and Gotsis A 2009 Permeability of polymer/clay nanocomposites: a review *Eur. Polym. J.* **45** 967–84
[27] Zhu J, Uhl F M, Morgan A B and Wilkie C A 2001 Studies on the mechanism by which the formation of nanocomposites enhances thermal stability *Chem. Mater.* **13** 4649–54
[28] Rafiee M A, Rafiee J, Wang Z, Song H, Yu Z-Z and Koratkar N 2009 Enhanced mechanical properties of nanocomposites at low graphene content *ACS nano* **3** 3884–90
[29] Tanaka T, Montanari G and Mulhaupt R 2004 Polymer nanocomposites as dielectrics and electrical insulation-perspectives for processing technologies, material characterization and future applications *IEEE Trans. Dielectr. Electr. Insul.* **11** 763–84
[30] Saravanan S, Gupta S, Ramamurthy P C and Madras G 2014 Effect of silane functionalized alumina on poly(vinyl butyral) nanocomposite films: thermal, mechanical, and moisture barrier studies *Polym. Compos.* **35** 1426–35
[31] Gupta S, Sindhu S, Varman K A, Ramamurthy P C and Madras G 2012 Hybrid nanocomposite films of polyvinyl alcohol and ZnO as interactive gas barrier layers for electronics device passivation *RSC Adv.* **2** 11536–43
[32] Gupta S, Seethamraju S, Ramamurthy P C and Madras G 2013 Polyvinylbutyral based hybrid organic/inorganic films as a moisture barrier material *Ind. Eng. Chem. Res.* **52** 4383–94
[33] Sitharaman B, Shi X, Walboomers X F, Liao H, Cuijpers V, Wilson L J, Mikos A G and Jansen J A 2008 *In vivo* biocompatibility of ultra-short single-walled carbon nanotube/biodegradable polymer nanocomposites for bone tissue engineering *Bone* **43** 362–70
[34] Satarkar N S, Biswal D and Hilt J Z 2010 Hydrogel nanocomposites: a review of applications as remote controlled biomaterials *Soft Matter* **6** 2364–71
[35] Ahuja T and Kumar D 2009 Recent progress in the development of nano-structured conducting polymers/nanocomposites for sensor applications *Sensors Actuators* B **136** 275–86
[36] Arora A and Padua G 2010 Review: nanocomposites in food packaging *J. Food Sci.* **75** R43–9
[37] Lange J and Wyser Y 2003 Recent innovations in barrier technologies for plastic packaging—a review *Packag. Technol. Sci.* **16** 149–58
[38] Seethamraju S, Ramamurthy P C and Madras G 2014 Performance of an ionomer blend-nanocomposite as an effective gas barrier material for organic devices *RSC Adv.* **4** 11176–87
[39] Choudalakis G and Gotsis A D 2009 Permeability of polymer/clay nanocomposites: a review *Eur. Polym. J.* **45** 967–84
[40] Bharadwaj R K 2001 Modeling the barrier properties of polymer-layered silicate nanocomposites *Macromolecules* **34** 9189–92
[41] Hegde M S, Madras G and Patil K C 2009 Noble metal ionic catalysts *Acc. Chem. Res.* **42** 704–12
[42] Rajeshwar K and de Tacconi N R 2009 Solution combustion synthesis of oxide semiconductors for solar energy conversion and environmental remediation *Chem. Soc. Rev.* **38** 1984–98
[43] Nagaveni K, Hegde M, Ravishankar N, Subbanna G and Madras G 2004 Synthesis and structure of nanocrystalline TiO_2 with lower band gap showing high photocatalytic activity *Langmuir* **20** 2900–7
[44] Daya Mani A, Rama Raju B, Xanthopoulos N, Ghosal P, Sreedhar B and Subrahmanyam C 2013 Effect of fuels on combustion synthesis of TiO_2—Towards efficient photocatalysts for methylene blue oxidation and Cr (VI) reduction under natural sunlight *Chem. Eng. J.* **228** 545–53
[45] Gupta S, Ramamurthy P C and Madras G 2011 Synthesis and characterization of flexible epoxy nanocomposites reinforced with amine functionalized alumina nanoparticles: a potential encapsulant for organic devices *Polym. Chem.* **2** 221–8
[46] Zhang L, Chen L, Wan H, Chen J and Zhou H 2011 Synthesis and tribological properties of stearic acid-modified anatase (TiO_2) nanoparticles *Tribol. Lett.* **41** 409–16
[47] Seethamraju S, Ramamurthy P C and Madras G 2013 Ionomer based blend as water vapor barrier material for organic device encapsulation *ACS Appl. Mater. Interfaces* **5** 4409–16
[48] Coates J 2000 Interpretation of infrared spectra, a practical approach *Encyclopedia of Analytical Chemistry* (New York: Taylor and Francis)
[49] Gupta S, Ramamurthy P C and Madras G 2011 Covalent grafting of polydimethylsiloxane over surface-modified alumina nanoparticles *Ind. Eng. Chem. Res.* **50** 6585–93
[50] Mueller R, Kammler H K, Wegner K and Pratsinis S E 2003 OH surface density of SiO_2 and TiO_2 by thermogravimetric analysis *Langmuir* **19** 160–5
[51] McIntosh K R, Cotsell J N, Cumpston J S, Norris A W, Powell N E and Ketola B M 2009 An optical comparison of silicone and EVA encapsulants for conventional silicon PV modules: a ray-tracing study *2009 34th IEEE Photovoltaic Specialists Conf.* (*PVSC*) pp 000544–9
[52] Schuller S, Schilinsky P, Hauch J and Brabec C J 2004 Determination of the degradation constant of bulk heterojunction solar cells by accelerated lifetime measurements *Appl. Phys.* A **79** 37–40